Femtosecond laser excitation of coherent optical phonons in ferroelectric $LuMnO_3$

Shi-Tao Lou, Frank M. Zimmermann, Robert A. Bartynski, Namjung Hur, and Sang-Wook Cheong
Department of Physics and Astronomy, Rutgers University, Piscataway, New Jersey 08854, USA
(Received 15 June 2008; revised manuscript received 28 April 2009; published 9 June 2009)

We have used femtosecond pump-probe spectroscopy to excite and probe coherent optical phonon vibrations in single crystals of hexagonal ferroelectric $LuMnO_3$. An optical phonon mode of A_1 symmetry was coherently excited with 25 fs pump-laser pulses ($\lambda \approx 800$ nm). The phonon mode, involving Lu ion motion along the c axis, was identified as the soft mode driving the ferroelectric transition. The excitation mechanism was determined to be purely displacive in nature due to resonant excitation of a narrow intra-atomic $d_{xy,x^2-y^2} \rightarrow d_{3z^2-r^2}$ transition in Mn. The lifetime of the Mn $d_{xy,x^2-y^2} \rightarrow d_{3z^2-r^2}$ excitation was measured to be 0.8 ps. A remarkable reversal of the sign of the oscillation amplitude (π phase shift) of the reflectivity curve was observed upon comparing longitudinal-optical (LO) with transverse-optical (TO) mode geometries. The phase reversal is attributed to the macroscopic electric depolarization field accompanying infrared-active longitudinal phonon modes but absent in TO modes. In addition to the direct effect of the ion motion on the optical properties, which is the same in LO and TO modes, the longitudinal depolarization field of the LO mode gives rise to an additional modulation of the refractive index via the linear electro-optic effect which dominates the optical response.

DOI: 10.1103/PhysRevB.79.214301 PACS number(s): 77.90.+k, 63.20.−e

I. INTRODUCTION

The hexagonal rare-earth manganites $RMnO_3$ (R=Ho, Er, Tm, Yb, Lu, and Y) are multiferroic materials in which magnetic order can coexist with ferroelectricity.[1,2] Magnetoelectric coupling between ferroelectric and magnetic orders in multiferroic materials[3] provides a novel avenue for controlling magnetization and magnetic domains by means of applied electric fields, promising exciting potential applications.[4,5] A clear understanding of the interactions between charge, orbital, spin, and lattice degrees of freedom is necessary to take advantage of these intriguing possibilities, and despite much progress in this direction, many questions remain. Certain phonon modes in $LuMnO_3$ exhibit an anomalous blueshift associated with the Néel transition into the antiferromagnetic phase due to spin-phonon interaction.[6] At room temperature, the hexagonal rare-earth manganites do not exhibit magnetic order due to geometric frustration in a triangular lattice.[4,7–16] Interactions between the nonmagnetic (electron and lattice) degrees of freedom give rise to high-temperature symmetry-changing phase transitions.[17–19] Ferroelectricity in $YMnO_3$ is induced by an unstable distortion mode (of symmetry K_3) which triples the unit cell and breaks inversion symmetry but which by itself does not induce a ferroelectric polarization to first order in the mode displacement, as it is a Brillouin-zone-boundary mode with zero uniform polarity.[18] Due to the lower symmetry at finite displacements of this distortion mode, coupling occurs to a second polar mode (Γ_2^- symmetry), which induces ferroelectricity. The ferroelectric polarization in this and similar materials is thus a secondary order parameter, driven by coupling of the polarization to the unstable nonpolar K_3 mode.[18] Understanding the relationship of these static distortion modes to dynamical phonon modes is required for a mechanistic description of the soft-mode driven ferroelectric phase transition.

In order to address this relationship, and to gain insight into the electron-phonon interactions in this class of materials, we have investigated the dynamics of coherently excited optical phonon vibrations in $LuMnO_3$ single crystals. Using time-resolved optical pump-probe spectroscopy, we have probed the photoinduced changes in the reflectivity $\Delta R/R$ at a photon energy of 1.55 eV (both pump and probe beams). This photon energy is near the center of a sharp absorption peak due to an intra-atomic optical transition involving the crystal-field split d levels of the Mn ion (the $d_{xy,x^2-y^2} \rightarrow d_{3z^2-r^2}$ transition of Mn^{3+}).[6] The reflectivity as measured by the probe beam (polarized in the direction of the $d_{xy,x^2-y^2} \rightarrow d_{3z^2-r^2}$ transition dipole) shows a sharp drop at zero pump-probe delay due to electronic excitation by the pump beam, followed by an exponential decay with a $\sim$0.8 ps time constant back to the equilibrium value, which is interpreted as a consequence of the lifetime of the $d_{xy,x^2-y^2} \rightarrow d_{3z^2-r^2}$ excitation. Observed oscillations in the reflectivity curves at a frequency of 3.6 THz are attributed to an optical phonon mode of A_1 symmetry. The phonon mode is coherently excited and exhibits dephasing with a time constant of about 5 ps. The initial phase of the reflectivity oscillations indicates that the excitation mechanism is purely displacive. Remarkably, the initial oscillation phases for longitudinal-optical (LO) and transverse-optical (TO) geometries differ by π. This is attributed to refractive-index modulation via the linear electro-optic effect by the macroscopic depolarization field accompanying LO phonons but absent in TO modes.

II. EXPERIMENT

Single crystals of $LuMnO_3$ were grown using Bi_2O_3 flux in a Pt crucible. The flux was held at 1280 °C for 5 h and slowly cooled down to 930 °C at a rate of 2 °/h. Hexagonal crystals grew in the form $\sim$0.1-mm-thick platelets with large (0001) (ab) facets, which cleaved into pieces of 3–5 mm size. Two crystal faces were studied: the ab (0001) face, which was used as grown, and the $(01\bar{1}0)$ face, given by the

perpendicular cleavage plane, which we call the *ac* face. The light source was a mode-locked Ti:sapphire laser with a center wavelength of 800 nm, providing ~25 fs pulses with a pulse energy on the order of 1 nJ at a repetition rate of 80 MHz. Extracavity pulse compression was performed in a prism pair to compensate for group-velocity dispersion in various optical elements. The laser beam was split into a pump beam (85%) and a probe beam (15%). The delay time between pump and probe pulses was ramped linearly, at a rate of 4 ps/s, by a fast scanning optical delay line (Clark MXR ODL-150). The pump-beam intensity was modulated at a frequency of 27 kHz by reflecting it from a piezoelectrically activated oscillating mirror, followed by passage of the focused beam through a narrow slit. A spherical metallic mirror (25 cm focal length) was used to focus both beams onto the same spot on the sample, resulting in an irradiated spot of about 75 μm diameter. For each beam, the angle of incidence with respect to the surface normal, as well as the angle with respect to the other beam, was about 5°. The pump-probe cross-correlation trace was measured by coupling out a portion of both beams with a beam splitter after the focusing mirror and focusing them onto a GaAsP photodiode. The one-photon sensitivity of the photodiode had a sharp drop off at 500 nm and complete long-wavelength cutoff at 600 nm due to the GaAsP band gap of ~2.5 eV. The nonlinear two-photon absorption signal was used to obtain the autocorrelation trace as a function of pump-probe delay time. The peak of the autocorrelation trace defined the zero of delay time, and deconvolution of the autocorrelation peak, assuming a $\mathrm{sech}^2(t)$ pulse shape, gave the full-width-at-half-maximum (FWHM) pulse width of approximately 25 fs. After passing a polarization analyzer, the reflected probe beam was detected with a shot-noise limited differential photodetector, which subtracted the intensity of a reference beam to eliminate laser noise. A lock-in amplifier was used to pick out the component of the signal modulated at the pump-beam modulation frequency. Pump-probe spectra were obtained by signal averaging of $\sim 10^5$ scan traces of the optical delay line. Experiments were performed in air at room temperature.

III. RESULTS AND DISCUSSION

In Fig. 1 we show the pump-probe spectra obtained for various geometries, plotting the relative reflectivity change as a function of pump-probe delay. Curves (a) and (b) correspond to reflection from the (0001) face (*ab* face) while curves (c) and (d) correspond to the $(01\bar{1}0)$ face (*ac* face). In curves (a) and (c) the pump and probe beams were perpendicularly polarized, whereas they were parallel in curves (b) and (d). The sharp spike at zero delay in curves (b) and (d) (peaking at approximately -6×10^{-4}, off the scale in the figure) is due to modulation of the reflectivity by the simultaneous irradiation of the sample by the pump pulse (coherent optical Kerr effect).[20] Interference at the detector between scattered pump light and the reflected probe beam also contributes to this spike for parallel polarization geometries. However, since the relative optical phases of the pump and probe beams drift randomly over the course of this type of

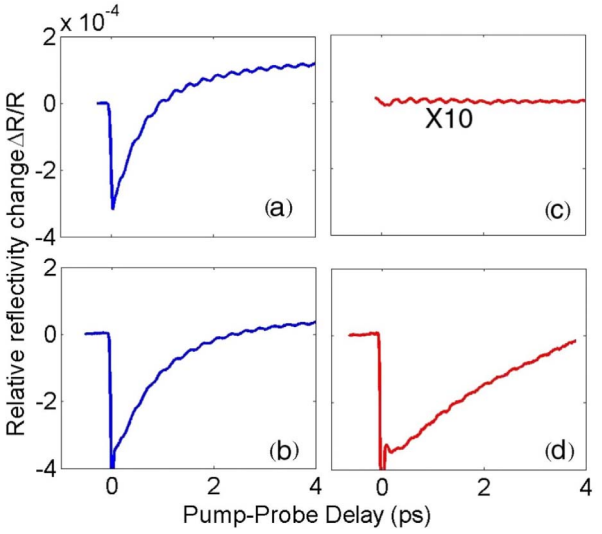

FIG. 1. (Color online) Pump-probe spectra of single crystal $LuMnO_3$ for different excitation and probe geometries. Curve (a) was measured by reflection of pump and probe beams from the *ab* (0001) face (near-normal incidence), with perpendicular polarization of pump and probe beams. Curve (b) was measured with the same laser beam propagation geometry as curve (a) but with parallel polarization of pump and probe beams. Curve (c) corresponds to reflection from the *ac* $(01\bar{1}0)$ face (near-normal incidence), with pump- and probe-beam polarizations perpendicular and parallel to the *c* axis, respectively. The amplitude of curve (c) is magnified ten times. Curve (d) shows the pump-probe spectrum again for reflection from the *ac* face but with both pump- and probe-beam polarizations perpendicular to the *c* axis.

experiment (without using a phase-lock loop), this pump-probe interference signal tends to cancel after extensive signal averaging, contributing only increased noise at zero delay. In curves (a), (b), and (d), a sharp drop in reflectivity at zero delay is followed by a more gradual decay back to the equilibrium reflectivity. This is interpreted as a transient optical bleaching effect due to partial saturation of the Mn $d_{xy,x^2-y^2}\rightarrow d_{3z^2-r^2}$ transition. In $LuMnO_3$, the Mn ions are surrounded by two apical and three in-plane oxygen ions.[14] The site symmetry of Mn is approximately D_{3h} (corresponding to the exact Mn site symmetry in the prototypical paraelectric high-temperature phase). In the crystal field, the Mn *d* orbitals thus split into three levels: E'' $(d_{xz,yz})$, E' (d_{xy,x^2-y^2}), and A_1' $(d_{3z^2-r^2})$ in order of increasing energy.[6] The $d_{xy,x^2-y^2}\rightarrow d_{3z^2-r^2}$ transition is one-photon allowed and gives rise to a sharp absorption peak centered at 1.58 eV,[6] coinciding with our laser's photon energy spectrum, centered at 1.55 eV. Since the transition dipole moment for this transition is perpendicular to the *c* axis, no such transient bleaching effect is expected for a geometry in which either pump or probe beams are polarized along the *c* axis, in agreement with the lack of any observed reflectivity drop in curve (c), and the absence of any observable signal when the pump beam was polarized parallel to the *c* axis (not shown). The excitation giving rise to the transient bleaching signal thus maintains some memory of the polarization of the exciting laser beam. We interpret the measured decay time of the reflectivity

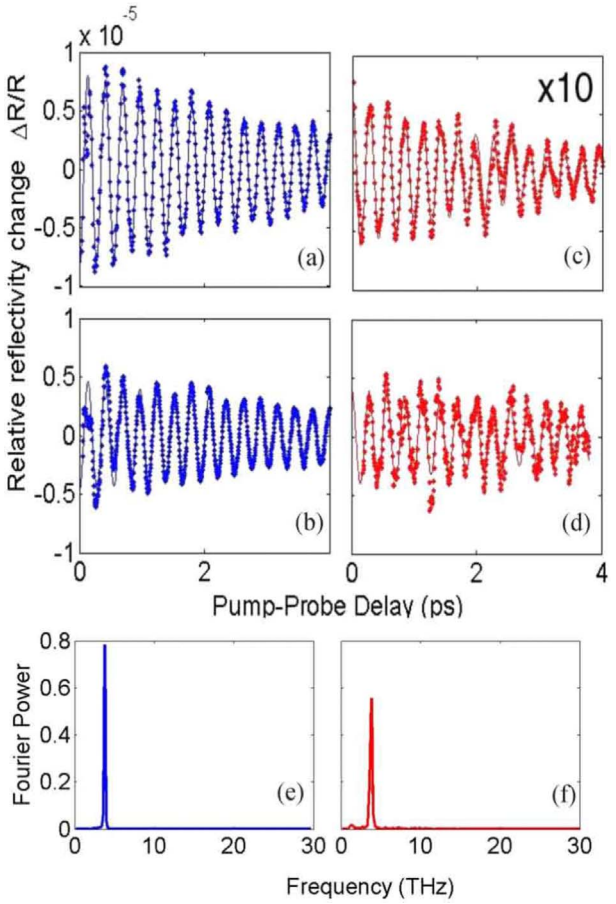

FIG. 2. (Color online) Oscillatory component of the reflectivity curves of Fig. 1. Curves (a) and (b) (acquired from the *ab* face) have the frequency of 3.61 THz, and the initial phase is very close to π. Curves (c) and (d) (acquired from the *ac* face) have a frequency of 3.54 THz, with an initial phase close to zero. In each graph, the continuous line is a fit to a decaying cosine oscillation (see text). Panels (e) and (f) show the Fourier power spectrum of the data shown in panels (b) and (d), respectively.

change of 0.8 ± 0.2 ps as the lifetime of the Mn $d_{xy,x^2-y^2} \rightarrow d_{3z^2-r^2}$ exciton at $T \approx 293$ K.

All curves in Fig. 1 show a pronounced oscillatory component, with a frequency characteristic of optical phonon modes. The oscillatory component of all curves is shown in Fig. 2, after subtraction of the slowly varying (primarily electronic) response. Fits of an exponentially decaying cosine function of the form $A\cos(2\pi ft-\varphi)\exp(-\gamma t)$ to the data are also plotted in the figure. The oscillation frequency for all spectra corresponding to reflection from the *ab* face was in this way measured to be 3.61 ± 0.02 THz (120 cm^{-1}) while the frequency corresponding to reflection of the *ac* face was 3.54 ± 0.02 THz (118 cm^{-1}). The decay time of the oscillation amplitude (phonon dephasing time γ^{-1}) was approximately 4 ps for all geometries. The initial phase of the oscillation was measured as $\varphi=(0.96 \pm 0.05)\ \pi$ for reflection from the *ab* face, and $\varphi=(0.00 \pm 0.03)\ \pi$ for reflection from the *ac* face. The fact that the initial phase of the phonon oscillation was close to zero or π indicates a displacive excitation mechanism.[21] In particular, we propose that the phonon mode is coherently excited due to a sudden shift in the equilibrium position of the phonon displacement coordinate upon excitation of the Mn $d_{xy,x^2-y^2} \rightarrow d_{3z^2-r^2}$ transition. This interpretation is consistent with an observed optical selection rule: in order to excite the phonon oscillation, the polarization of the pump beam must have a component in the *ab* plane, i.e., along the transition dipole of the Mn $d_{xy,x^2-y^2} \rightarrow d_{3z^2-r^2}$ transition.

In order to determine the symmetry of the observed phonon modes, we performed a polarization/symmetry analysis. Since we measured modulations in the reflectivity caused by motions in the phonon displacement coordinate, which are related to refractive-index modulations, our measurement is sensitive only to those modes where the refractive index has a first-order dependence on the phonon displacement. The derivative of the polarizability with respect to the phonon displacement coordinate is the Raman tensor; thus we can only probe Raman-active modes. Ferroelectric $LuMnO_3$ has space-group $P6_3cm$, with point group C_{6v}. Since we used a coherent optical probe, with a light wavelength that is much greater than the unit-cell dimensions, the measurement is sensitive only to phonon modes near the Γ point ($\mathbf{q} \approx 0$). Phonon modes at $\mathbf{q}=0$ can be classified according to the C_{6v} point-group symmetries, with irreducible representations A_1, A_2, B_1, B_2, E_1, and E_2. Of these, modes of A_1, E_1, and E_2 symmetries are Raman active, A_1 and E_1 are infrared active while A_2, B_1, and B_2 are silent modes.

The C_{6v} Raman-active modes have Raman tensors of the form

$$A_1:\begin{pmatrix} a & & \\ & a & \\ & & b \end{pmatrix},$$

$$E_1(x):\begin{pmatrix} & & c \\ & & \\ c & & \end{pmatrix}, E_1(y):\begin{pmatrix} & & \\ & & c \\ & c & \end{pmatrix},$$

$$E_2(xy):\begin{pmatrix} & d & \\ d & & \\ & & \end{pmatrix}, E_2(x^2-y^2):\begin{pmatrix} d & & \\ & -d & \\ & & \end{pmatrix}, \quad (1)$$

where the z direction is along the crystallographic c axis while the x and y axes are in the *ab* plane, and without loss of generality we choose the x axis by the projection of the polarization direction of the pump beam onto the *ab* plane. All data shown in Figs. 1 and 2 were recorded with the polarization analyzer parallel to the probe-beam polarization, which in all cases is along one of the Cartesian axes. Therefore, in these geometries the oscillatory component of the signal probes a diagonal element of the Raman tensor. Specifically, panel (a) of Fig. 2 shows an oscillation due to the *yy* element, panel (b) probes the *xx* element, panel (c) probes the *zz* element, and panel (d) again probes the *xx* element of the Raman tensor. The oscillation probed by reflection from the *ab* face [Figs. 2(a) and 2(b)] can thus only be due to a phonon mode of A_1 or $E_2(x^2-y^2)$ symmetry since these are the only symmetries with diagonal Raman tensor elements. Furthermore, $E_2(x^2-y^2)$ can be excluded since the oscilla-

TABLE I. Shell model parameters. Here, Z is the ionic charge, Y is the charge of the massless shell, and k is the coupling force constant between the core and its shell. The parameters a, b, and C are the constants of the Born-Mayer-Buckingham short-range potential of form $a\exp(-br)-\frac{C}{r^6}$.

Ion	Z ($\|e\|$)	Y ($\|e\|$)	k (eV/Å^2)	Ionic pair	a (eV)	b (Å)	C (eV Å^6)
Lu	2.85	1.7	50.45	Lu-O	1668	0.3262	0
Mn	2.85	3.0	35.98	Mn-O	1928	0.2959	0
O	−1.9	−3.0	60.80	O-O	22764	0.14901	20.37

tions of Figs. 2(a) and 2(b) are in phase while the $E_2(x^2-y^2)$ Raman tensor predicts them to have opposite phases. We conclude that the phonon oscillation observed in panels (a) and (b) of Figs. 1 and 2 is totally symmetric (A_1 symmetry). Similarly, the probe-beam polarization ensures that the oscillation of Fig. 2(d) is due to the xx element of the Raman tensor, which rules out all symmetries except for A_1 and $E_2(x^2-y^2)$. Moreover, since the oscillation of Fig. 2(c) probes the zz element, all symmetries except for A_1 may be ruled out. Therefore, the oscillation excited by the pump-beam geometry of panels (c) and (d) of Figs. 1 and 2 is also of A_1 symmetry. Other experiments with the probe-beam polarization at 45° with respect to the Cartesian axes, probing the off-diagonal elements of the Raman tensor (data not shown), confirm these symmetry assignments.

Despite the fact that the symmetry of all observed phonon modes is A_1, and in all cases the cosinelike initial phase of the oscillation implies a displacive excitation mechanism,[21,22] we note important differences. Specifically, comparing the oscillations measured by reflection from the ab face [panels (a) and (b) in Figs. 1 and 2] with those measured from the ac face [panels (c) and (d) in Figs. 1 and 2], we observe that the frequency of the ac-face oscillation is about 2 cm^{-1} lower, and the initial phases of the oscillation are opposite: the ab-face oscillation starts out with a negative reflectivity change while the ac-face oscillation starts out with an enhanced reflectivity. This is especially remarkable when comparing Figs. 2(b) and 2(d) since both pump-beam and probe-beam polarization directions were the same in both experimental geometries, implying that both experiments probed modulation of the same component (the ordinary ray) of the anisotropic refractive index.

To gain insight into the atomic motions underlying the observed oscillations, we simulated the lattice dynamics of the $LuMnO_3$ crystal with a shell model,[24] with crystal structure parameters from Refs. 14 and 25. Shell model parameters, adapted from Refs. 26 and 27, are listed in Table I. The model reproduces the measured infrared phonon frequencies[6] quite well, as shown in Table II. Further confidence in the validity of the shell-model calculation is obtained by comparing the calculated frequencies and phonon eigenvectors with those calculated by state-of-the-art first-principles calculations.[23] The lowest frequency A_1 modes predicted by the shell model [124 cm^{-1} for LO and 123 cm^{-1} for TO polarizations] are close to the observed coherent phonon frequencies of 120 and 118 cm^{-1}, respectively. The calculated phonon eigenvectors of the LO and TO modes are essentially identical. Both involve primarily motion of the Lu1 and Lu2 ions with opposite phases along the c axis, as shown in Fig. 3. This phonon eigenvector resembles the static distortion that the crystal undergoes when going from the prototypical high-temperature $P6_3/mmc$ phase to the ferroelectric $P6_3cm$ phase. To quantify this resemblance, we project the static distortion onto the calculated phonon eigenvectors of A_1

TABLE II. Calculated and experimental phonon frequencies of A_1 symmetry modes, and the squared projection of the calculated phonon eigenvectors onto the static distortion mode of the ferroelectric $P6_3cm$ structure (with respect to the prototypic $P6_3/mmc$ structure). The numbers in the projection column thus indicate the proportion of the static distortion mode that is given by the various phonon eigenvectors. Also indicated is the dominant atomic displacement of the calculated LO modes. The experimental frequencies are from infrared-absorption data by Souchkov *et al.* (Ref. 6) at 300 K.

Calculated frequency (cm^{-1})		Measured frequency (cm^{-1})	Projection onto static distortion		
LO	TO	TO	LO	TO	Largest atomic displacement
124	123	119	0.800	0.814	$+z$(Lu1),$-z$(Lu2)
251	208	223	0.014	0.035	$+z$(Mn),$-z$(Lu1)
267	260	261	0.124	0.030	Rot$_{xy}$(MnO_5)
283	280	295	0.042	0.101	x(Mn),z(O3)
421	393		0.013	0.000	z(O3,O4)
460	435		0.003	0.016	$+z$(Mn),$-z$(O3,O4)
475	472	478	0.000	0.000	x,y(O1,O2),$-z$(O3)
620	591	568	0.003	0.002	$+z$(Mn,O3,O4),$-z$(O1,O2)
676	676		0.002	0.002	$+z$(O1),$-z$(O2)

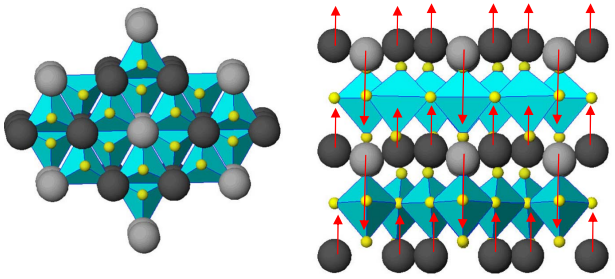

FIG. 3. (Color online) Schematic of the $P6_3cm$ crystal structure of ferroelectric $LuMnO_3$. On the left is the view approximately along the c axis, and on the right is a side view, along the ab planes. The triangular bipyramids represent MnO_5 units, with oxygen ions at each apex and a Mn ion at the center. Two inequivalent Lu ions, designated Lu1 and Lu2, are represented by light and dark gray balls, respectively. The coherently excited A_1 phonon mode primarily involves Lu1 and Lu2 ions oscillating along the c axis, as shown by the red arrows. The phonon eigenvector is similar to the static distortion of the lattice with respect to the prototypic $P6_3/mmc$ structure.

symmetry, also shown in Table II. The static distortion is composed of approximately 80% of the calculated eigenvector of the 123 and 124 cm^{-1} phonons, with higher frequency A_1 modes providing the remaining 20%. We conclude that the coherently excited phonon mode is the lowest frequency totally symmetric (A_1) mode, which is the dominant component of the soft mode mediating the transition from the prototypic $P6_3/mmc$ phase to the ferroelectric $P6_3cm$ phase.

The instability driving this transition, as well as the source of ferroelectricity, were studied by Fennie and Rabe[18] in the isostructural compound $YMnO_3$, using first-principles density-functional calculations. They identified atomic motions along two normal-mode coordinates of different symmetries, labeled Γ_2^- and K_3, according to the irreducible representations of the prototypic $P6_3/mmc$ space group. The dynamic instability was identified as a K_3 symmetry mode, which is a unit-cell tripling Brillouin-zone-boundary (K-point) mode involving buckling of the Y (Lu) ionic planes and rotation of the MnO_5 polyhedra. The distorted structure is shown in Fig. 3. Although distortion along the K_3 coordinate breaks inversion symmetry, as a zone-boundary mode, the K_3 mode is nonpolar. This means that the ferroelectric polarization associated with distortion along this coordinate is zero to first order in the distortion (the Born effective charges are zero) but third order (and higher odd order) terms give rise to polarization for finite mode displacements. Furthermore, in a state of finite distortion along the unstable K_3 coordinate, the symmetry is reduced to $P6_3cm$, enabling the K_3 mode to couple to polar Γ_2^- modes since both K_3 and Γ_2^- transform according to the same totally symmetric (Γ_1) irreducible representation ($\mathbf{q}=0$ and A_1 point-group symmetry) in the $P6_3cm$ space group. In order to relate the coherent phonon mode observed in our experiment to these static distortion modes, we decompose both the static distortion and the calculated phonon eigenvectors into symmetry components corresponding to the prototypic $P6_3/mmc$ structure. The result is shown in Table III. The static distortion turns out to exhibit predominantly the symmetry of the unstable K_3 mode (98%) and only a small admixture of polar Γ_2^- modes (2%). Similarly, the calculated coherent phonon eigenvector consists of 99% K_3 and less than 1% Γ_2^-. We conclude that the coherent phonon is essentially motion along the nonpolar K_3 soft-mode coordinate that drives the ferroelectric transition, with a small amount of admixture of the polar Γ_2^- mode.

Although small, the polar Γ_2^- component of the phonon eigenvector has important consequences. This small polar component renders the mode infrared active and is furthermore responsible for a small frequency splitting between the LO and TO propagation geometries. This is due to the additional restoring force exerted on the ions by the electric depolarization field present in the longitudinal case, resulting in a higher phonon frequency than the transverse mode, which does not exhibit such a depolarization field. As the electric polarization of both modes is along the c axis, the LO geometry corresponds to phonon propagation ($\mathbf{q}$ vector) along the c axis, and the TO geometry corresponds to perpendicular propagation ($\mathbf{q}$ in the ab plane). The coherent phonon excited in our experiment does not have a well-defined $\mathbf{q}$ vector since the phonon oscillation is excited only in the thin slab of crystal near the surface where the pump-laser beam is absorbed. The thickness of the slab is determined by the optical-absorption depth (estimated to be of the order of tens of nanometers). Confinement of the phonon oscillation to a thin slab (with slab thickness $\gg$ lattice constant) results in a distribution of $\mathbf{q}$ vectors along a short "rod" in reciprocal space, perpendicular to the surface plane, passing through $\mathbf{q}=0$.[22] The length Δq of this rod is of the order of the optical-absorption coefficient, which, due to the strong absorption resonance, is expected to be greater than the laser photon wave number, which itself is much greater than the wave number of a photon at the TO phonon frequency, where the TO phonon and the photon dispersion curves exhibit an avoided crossing (phonon-polariton modes). Our experiment thus sample a range of phonon wave vectors around the $\mathbf{q}=0$ point, with average magnitudes that greatly exceed the very limited range where the phonon modes have polariton (mixed photon-phonon) character. We therefore ignore phonon-polariton effects in our analysis. Given such a rodlike distribution of $\mathbf{q}$ vectors, we may distinguish between LO and TO polarization geometries, depending on whether this rod is along the c axis (for near-normal reflection from the ab face) or perpendicular to it (for near-normal reflection from the ac face). This relationship is illustrated schematically in Fig. 4. When the pump-laser beam (red arrow) is reflected from the ab face, the excited coherent phonon motion is confined to a thin slab perpendicular to the c axis. Since the polarization of the excited coherent phonon is along the c axis, an LO phonon geometry results, in which the dynamical phonon polarization is accompanied by an opposing electric depolarization field, oscillating at the phonon frequency. When the laser beam is reflected from the ac face, on the other hand, the excited slab is parallel to the c axis. Since the phonon polarization is now parallel to the slab, a TO geometry results, in which the depolarization field is primarily outside of the slab, and becomes negligible in the limit of large aspect ratio of the slab. As predicted by these considerations, we find the coherent phonon frequency for ab-face reflection (LO polarization) slightly higher than the

TABLE III. Decomposition of the static distortion mode in the ferroelectric $P6_3cm$ structure (Ref. 25) (with respect to the prototypic $P6_3/mmc$ structure, where most atomic positions are fixed by symmetry) on the one hand, and the calculated 123 cm^{-1} TO phonon eigenvector on the other, into irreducible representations of the $P6_3/mmc$ space group. Γ_1^+ and Γ_2^- are Brillouin-zone-center modes while K_1 and K_3 are unit-cell tripling Brillouin-zone-boundary modes. Ferroelectric polarization is primarily due to distortions of Γ_2^- symmetry, which is the only polar symmetry involved. In order to directly compare these modes, both the static distortion mode and the phonon eigenvector (given in columns labeled "Total") are expressed as atomic displacements, weighted by the square root of the atomic mass, and normalized to unity upon summation over all 30 atoms in the $P6_3cm$ unit cell. The decomposition of these eigenvector components into modes of $P6_3/mmc$ symmetry is shown in the following columns. Blank entries correspond to values that are zero by symmetry. The magnitude of the static displacement in the totally symmetric Γ_1^+ mode (involving only z motion of the apical oxygen ions O1 and O2) is unknown, and was set to zero since totally symmetric displacements are not constrained by symmetry in the high-symmetry structure, and no experimental structural data are available for the high-temperature $P6_3/mmc$ phase. The row labeled "Weight" gives the sum of the squares of the numbers in the respective columns over all 30 atoms in the unit cell. It indicates that the static distortion mode and the calculated phonon mode consist of 98% and 99% K_3 character, respectively. The decomposition of the 124 cm^{-1} LO phonon eigenvector (not shown) is essentially the same as that of the TO phonon.

	Static distortion					Calculated phonon eigenvector				
	Total	Γ_1^+	Γ_2^-	K_1	K_3	Total	Γ_1^+	Γ_2^-	K_1	K_3
Lu1(z)	0.485		−0.035		0.521	0.562		−0.013		0.576
Lu2(z)	−0.296		−0.035		−0.260	−0.301		−0.013		−0.288
Mn(x)	0.012			0.012		0.016			0.016	
Mn(z)	0.024		0.024			0.009		0.009		
O1(x)	−0.076			0.003	−0.079	−0.005			−0.005	0.000
O1(z)	0.019	−0.000	0.019			0.002	−0.002	0.004		
O2(x)	0.081			0.003	0.079	−0.005			−0.005	0.000
O2(z)	0.019	0.000	0.019			0.006	0.002	0.004		
O3(z)	−0.137		0.035		−0.172	0.033		0.019		0.014
O4(z)	0.121		0.035		0.086	0.012		0.019		−0.007
Weight	1.000	0.000	0.023	0.001	0.977	1.000	0.000	0.004	0.002	0.994

frequency for ac-face reflection (TO polarization) due to the additional restoring force provided by the LO depolarization field. The small magnitude of the observed LO-TO frequency splitting (approximately 2 cm^{-1}) is consistent with the small splitting predicted by the shell-model calculation, which is due to a weak mode polarity caused by the small Γ_2^--symmetry admixture to the nonpolar K_3 mode.

In addition to this slight difference in frequency, we observe a remarkable reversal of the initial phase of the oscillation. Specifically, if we extrapolate the oscillation to zero pump-probe delay, the relative reflectivity change $\Delta R/R$ at $t=0$ is negative in the LO geometry [Figs. 2(a) and 2(b)] while it is positive in the TO geometry [Figs. 2(c) and 2(d)]. Since the probe-beam geometries of Figs. 2(a), 2(b), and 2(d) are sensitive to modulations of the ordinary refractive index n_o [related to the Raman tensor element a in Eq. (1)], and only that of Fig. 2(c) is sensitive to modulations of the extraordinary index n_e [related to the Raman tensor element b in Eq. (1)], we can exclude the possibility that a difference in sign between Raman tensor elements a and b might be the origin of this phase reversal. In fact, the polarization directions of both pump and probe lasers were the same in Figs. 2(b) and 2(d), implying that the observed phase reversal can only be due to the difference in **q** vector [LO in Fig. 2(b), and TO in Fig. 2(d)]. Since the phonon eigenvectors (ionic displacements) are essentially identical for LO and TO geometries, the only remaining difference that can account for the phase reversal are static or dynamic electric depolarization fields that are present in the LO case but absent in the TO case.

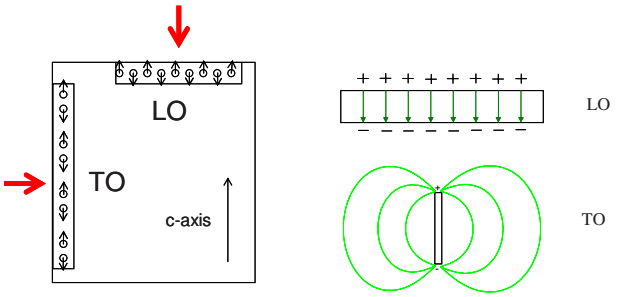

FIG. 4. (Color online) Schematic of longitudinal-optical (LO) and transverse-optical (TO) phonon motion geometries. The left panel shows the geometry of the pump-laser beam with respect to the crystallographic c axis. The right panel depicts the electric depolarization fields for polarized slabs with polarizations along the slab surface normal (LO) and perpendicular to it (TO).

We propose two possible scenarios for depolarization fields to affect the phase of the observed oscillation. In the first scenario, the phase of the phonon oscillation (the phase of the ion motion) excited by the pump pulse is reversed between LO and TO. In this scenario (which we call the pump-beam scenario), pump light absorption leads to a sudden change in the magnitude of the static ferroelectric polarization along the c axis due to a sudden change in electronic

state populations upon light absorption. In the LO geometry, this sudden change in polarization will be accompanied by a sudden change in depolarization field, which in turn couples to the electric polarization of the phonon mode, displacively exciting the infrared-active phonon via electric-field coupling. In the TO geometry, on the other hand, the sudden change in depolarization field is absent (because in this case, the static polarization, just like the phonon polarization, is along the slab, as sketched in Fig. 4), and phonon excitation can thus occur only by a mechanism involving changes in bond geometries directly induced by electronic excitation, not mediated by the macroscopic electric field. (This latter excitation mechanism applies to both LO and TO geometries, of course.) If the magnitude of the depolarization-field induced displacement (LO) of the equilibrium phonon coordinate is larger than that of the direct bonding-induced displacement (TO and LO), and the signs of the two displacements are opposite, the observed phase reversal will result. The pump-beam scenario thus predicts the oscillation phases of LO and TO modes to be reversed. In the second possible scenario (which we will call the probe-beam scenario), on the other hand, the phases of the phonon oscillation are the same for LO and TO modes but the reflectivity changes seen by the probe beam are reversed in sign. This could be due to the linear electro-optic effect (Pockels effect) present in noncentrosymmetric crystals such as $LuMnO_3$.[28] In both LO and TO geometries, the change in ion positions will directly modulate the refractive index via the Raman tensor. However, in the LO case only, the oscillating depolarization field will cause an additional modulation of the refractive index via the electro-optic effect. If the electro-optic modulation is larger than the direct Raman-type modulation, and the two modulations are opposite in sign, the observed phase reversal in the reflectivity will result. While we cannot definitively rule out either one of the two proposed scenarios, the probe-beam scenario seems more likely for the following reason. In the pump-beam scenario, the change in static depolarization field is expected to couple to all infrared-active modes. Since there are a number of phonon modes in the experimentally accessible frequency range for which the mode polarization is much larger than for the mode that is actually excited (as judged by the observed IR line intensities[6] and by the calculated LO-TO frequency splittings), we would expect such modes to be very efficiently excited by the field-coupling mechanism, in contrast to the single frequency observed in the Fourier transform (Fig. 2). In the probe-beam scenario, on the other hand, the excitation mechanism does not involve the macroscopic electric field, and it is thus possible that (for some as yet unknown reason) this excitation mechanism is strongly selective for the observed coherent phonon mode. Regarding the phonon excitation mechanism (beyond the fact that it is displacive), we may speculate that the Mn $d_{xy,x^2-y^2} \rightarrow d_{3z^2-r^2}$ transition is accompanied by some amount of electronic charge transfer from the in-plane oxygen ions (which couple more strongly to the Mn d_{xy,x^2-y^2} orbitals) to the apical oxygen (which couple more readily to the $d_{3z^2-r^2}$ orbital). Due to the crystal structure in the ferroelectric phase, such charge transfer would result in net changes in the electrostatic forces on the Lu1 and Lu2 ions leading to these ions' respective motions in opposite directions along the c axis, increasing the ferroelectric distortion, as in the coherently excited phonon mode. As this is no more than speculation, however, detailed theoretical investigations appear necessary to provide a thorough explanation of why optical excitation of the Mn $d_{xy,x^2-y^2} \rightarrow d_{3z^2-r^2}$ exciton selectively excites coherent oscillations along the soft-mode coordinate involved in the ferroelectric transition.

IV. CONCLUSION

In summary, we have used femtosecond pump-probe spectroscopy to elucidate the femtosecond and picosecond photoinduced dynamics of $LuMnO_3$ single crystal. Absorption of 25 fs pulses of 800 nm light, polarized perpendicularly to the c axis, excites the Mn $d_{xy,x^2-y^2} \rightarrow d_{3z^2-r^2}$ transition, which results in a transient reflectivity change for light of the same wavelength and polarization due to partial saturation of the transition. The electronic relaxation time is of the order of 1 ps. Furthermore, exciting this transition results in coherent excitation of an A_1-symmetry phonon (TO: 118 cm^{-1} and LO: 120 cm^{-1}) by a displacive mechanism. The phonon eigenvector, involving motion of the Lu1 and Lu2 ions along the c axis in opposite directions, is essentially the soft-mode coordinate involved in the ferroelectric transition. TO and LO phonon polarizations exhibit opposite initial phases of the reflectivity oscillation, which is attributed to modulation of the refractive index by the longitudinal depolarization field of the LO phonon via the linear electro-optic effect.

ACKNOWLEDGMENTS

We thank C. J. Fennie for useful discussions and sharing unpublished results. This work was supported by the National Science Foundation under Grant No. DMR-0304432 and the Department of Energy under Grant No. DE-FG-02-07ER46382.

[1] G. A. Smolenskii and I. E. Chupis, Sov. Phys. Usp. **25**, 475 (1982).
[2] S. C. Abrahams, Acta Crystallogr., Sect. B: Struct. Sci. **B57**, 485 (2001).
[3] W. Eerenstein, N. D. Mathur, and J. F. Scott, Nature (London) **442**, 759 (2006).
[4] M. Fiebig, T. Lottermoser, D. Frohlich, A. V. Goltsev, and R. V. Pisarev, Nature (London) **419**, 818 (2002).
[5] T. Lottermoser, T. Lonkai, U. Amann, D. Hohlwein, J. Ihringer, and M. Fiebig, Nature (London) **430**, 541 (2004).
[6] A. B. Souchkov, J. R. Simpson, M. Quijada, H. Ishibashi, N. Hur, J. S. Ahn, S. W. Cheong, A. J. Millis, and H. D. Drew,

Phys. Rev. Lett. **91**, 027203 (2003).
[7] A. Munoz, J. A. Alonso, M. J. Martinez-Lope, M. T. Casais, J. L. Martinez, and M. T. Fernandez-Diaz, Phys. Rev. B **62**, 9498 (2000).
[8] M. Fiebig, C. Degenhardt, and R. V. Pisarev, J. Appl. Phys. **91**, 8867 (2002).
[9] M. Fiebig, Th. Lottermoser, Th. Lonkai, A. V. Goltsev, and R. V. Pisarev, J. Magn. Magn. Mater. **290-291**, 883 (2005).
[10] M. Janoschek, B. Roessli, L. Keller, S. N. Gvasaliya, K. Conder, and E. Pomjakushina, J. Phys.: Condens. Matter **17**, L425 (2005).
[11] T. Katsufuji, S. Mori, M. Masaki, Y. Moritomo, N. Yamamoto, and H. Takagi, Phys. Rev. B **64**, 104419 (2001).
[12] T. Katsufuji, M. Masaki, A. Machida, M. Moritomo, K. Kato, E. Nishibori, M. Takata, M. Sakata, K. Ohoyama, K. Kitazawa, and H. Takagi, Phys. Rev. B **66**, 134434 (2002).
[13] O. P. Vajk, M. Kenzelmann, J. W. Lynn, S. B. Kim, and S.-W. Cheong, Phys. Rev. Lett. **94**, 087601 (2005).
[14] B. B. Van Aken, A. Meetsma, and T. T. M. Palstra, Acta Crystallogr., Sect. E: Struct. Rep. Online **E57**, i101 (2001).
[15] B. B. Van Aken, A. Meetsma, and T. T. M. Palstra, Acta Crystallogr., Sect. C: Cryst. Struct. Commun. **C57**, 230 (2001).
[16] B. B. Van Aken, T. T. M. Palstra, A. Filippetti, and N. A. Spaldin, Nature Mater. **3**, 164 (2004).
[17] B. B. Van Aken and T. T. M. Palstra, Phys. Rev. B **69**, 134113 (2004).
[18] C. J. Fennie and K. M. Rabe, Phys. Rev. B **72**, 100103(R) (2005).
[19] T. Lottermoser and M. Fiebig, Phys. Rev. B **70**, 220407(R) (2004).
[20] T. E. Stevens, J. Kuhl, and R. Merlin, Phys. Rev. B **65**, 144304 (2002).
[21] H. J. Zeiger, J. Vidal, T. K. Cheng, E. P. Ippen, G. Dresselhaus, and M. S. Dresselhaus, Phys. Rev. B **45**, 768 (1992).
[22] R. Merlin, Solid State Commun. **102**, 207 (1997).
[23] C. J. Fennie (unpublished).
[24] M. B. Taylor, G. D. Barrera, N. L. Allan, T. H. K. Barron, and W. C. Mackrodt, Comput. Phys. Commun. **109**, 135 (1998).
[25] B. B. Van Aken, A. Meetsma, and T. T. M. Palstra, Acta Crystallogr., Sect. C: Cryst. Struct. Commun. **C57**, 230 (2001).
[26] A. P. Litvinchuk, M. N. Iliev, V. N. Popov, and M. M. Gospodinov, J. Phys.: Condens. Matter **16**, 809 (2004).
[27] M. N. Iliev, H.-G. Lee, V. N. Popov, M. V. Abrashev, A. Hamed, R. L. Meng, and C. W. Chu, Phys. Rev. B **56**, 2488 (1997).
[28] A. V. Kuznetsov and C. J. Stanton, Phys. Rev. B **51**, 7555 (1995).